Nonlinear interfacial progressive waves near a boundary in a Boussinesq fluid

D.I. Pullin
Department of Mechanical Engineering, University of Queensland, St. Lucia, Queensland 4067, Australia
R. H. J. Grimshaw
Department of Mathematics, University of Melbourne, Parkville, Victoria 3052, Australia

(Received 4 May 1982; accepted 11 September 1982)

The behavior of nonlinear progressive waves at the interface between two inviscid fluids in the presence of an upper free boundary is studied as a model of waves on the thermocline. A set of relationships between the integral properties of bounded waves in a general two-fluid model is first developed and the Stokes expansion to third order is derived. The exact free boundary problem for the wave profile is then formulated within the Boussinesq approximation as a nonlinear integral equation, which is solved numerically using two different numerical methods. For finite velocity difference across the two-fluid interface bifurcation of solutions into upper and lower branch wave profiles with quite different properties is obtained. Numerically calculated wave shapes and integral properties show good agreement with third-order Stokes expansion predictions in the weakly nonlinear regime for waves which are not too long. Very long waves were found to exhibit distinct solitary wave-like features.

I. INTRODUCTION

The thermocline in lakes, fjords, and coastal waters and its counterpart, the inversion which caps the atmospheric boundary layer, are regions which support progressive internal gravity waves, e.g., Halpern,[1] Farmer,[2] or Christie, Muirhead, and Hales.[3] Often these waves produce vertical displacements of the thermocline comparable with the thermocline depth, indicating that nonlinear effects are significant. Further the thermocline is often associated with a basic shear flow with a velocity change across the thermocline comparable to the phase speed of the waves.

It is thus our purpose in this paper to obtain and study nonlinear solutions to a simple two-layer model of the thermocline in the Boussinesq limit in order to explore nonlinear effects associated with large wave amplitude. Several studies along these lines have appeared to date. Thorpe[4] conducted a comprehensive set of experiments and successfully compared his results with a Stokes expansion to the third order in the wave amplitude. Holyer[5] carried the Stokes expansion to very high order and calculated wave profile shapes for progressive waves moving at the interface between two deep fluids of different densities. Solutions for the Boussinesq limit were obtained as a special case. Vanden-Broeck[6] treated essentially the same class of flows with the inclusion of an interfacial surface-tension term using an exact integral equation formulation based on the use of the Hilbert transform. While the case where the upper fluid has finite depth does not seem to have been studied in detail, Hogan[7] has developed expressions for the wave integral properties in bounded fluids when there is no mean velocity difference across the interface. The effect of a basic shear flow on the interfacial waves has not been studied in the fully nonlinear case, although Nayfeh and Saric[8] derived the third-order Stokes expansion for the deep fluid case, and Thorpe[9] considered small amplitude waves both theoretically and experimentally.

In the present paper we consider large-amplitude progressive waves moving between fluids of different density and different mean velocities in the Boussinesq limit in which the density difference is neglected in all but the buoyancy terms of the equations of motion. We utilize a two-layer irrotational fluid model with an infinitely deep lower fluid and a finite depth upper fluid representing the thermocline. In the Boussinesq limit the effect of the free surface is modeled by a rigid plane.

In Sec. II we give expressions for the integral properties of general nonlinear progressive waves and derive the Stokes expansion to third order in the wave amplitude. The free boundary problem for the wave profile is considered in Sec. III, and the midpoint approximation and Fourier expansion methods of numerical solution are described. The respective analytical and numerical results are discussed briefly in Sec. IV.

II. ANALYTIC SOLUTIONS FOR PROGRESSIVE WAVES

A. Integral properties

We consider the passage of two-dimensional progressive waves of wavelength λ at the interface between two inviscid incompressible fluids. We work in rectangular coordinates (x,y) with the x axis aligned with the mean interface level. Acceleration due to gravity g acts in the negative y direction. Subscripts 1 and 2 denote fluid properties above and below the interface, respectively, and the fluid densities are ρ_1 and ρ_2 with $\rho_2 > \rho_1$. For present generality and later convenience, we consider a two-layer model bounded by solid horizontal planes $y = -d_2$ and $y = d_1$. In our arbitrary reference frame the wave phase speed is c, while the interface shape is denoted by $y = \eta(x,t)$ with zero mean. The flow is assumed to be irrotational and two-dimensional in each layer. We let ϕ_j be the velocity potential in each fluid ($j = 1,2$) and denote the velocity field by $u_j = \partial\phi_j/\partial x$ and

 0031-9171/83/040897-09$01.90

$v_j = \partial\phi_j/\partial y$. The boundary conditions are that

$$\left.\begin{aligned} v_1 &= 0, \text{ at } y = d_1, \\ v_2 &= 0, \text{ at } y = -d_2, \end{aligned}\right\} \tag{1}$$

$$\left.\begin{aligned} p_1 &= p_2, \\ \frac{\partial\eta}{\partial t} + \mathbf{u}_j\cdot\nabla\eta &= v_j, \quad j = 1,2 \end{aligned}\right\} \text{ on } \mathscr{C}, \tag{2}$$

where $\mathbf{u} = (u,v)$, $\mathscr{C}$ is one wavelength of the interface, and where $p_j, j = 1,2$ are the fluid pressures given by the Bernoulli equation

$$\frac{p_j}{\rho_j} + gy + \frac{\partial\hat{\phi}_j}{\partial t} + \frac{1}{2}u_j^2 + \frac{1}{2}v_j^2 = K_j + \frac{1}{2}\bar{u}_j^2, \quad j = 1,2. \tag{3}$$

In (3) K_j are Bernoulli constants. For periodic progressive waves we may further define

$$\text{“}\overline{}\text{”} = \frac{1}{\lambda}\int_0^\lambda \cdots dx, \tag{4}$$

$$\phi_j = \bar{u}_j x + \hat{\phi}_j, \tag{5}$$

$$\hat{u}_j = \frac{\partial\hat{\phi}_j}{\partial x} = u_j - \bar{u}_j, \tag{6}$$

$$\frac{\partial}{\partial t} = -c\frac{\partial}{\partial x}. \tag{7}$$

Equation (4) defines the mean over a single wavelength while in (5), $\hat{\phi}$ is periodic with zero mean. Equation (7) applies generally to all variables except those mean quantities such as $\bar{u}_j x$ in (5).

Using (1), (3), and (4)–(7) together with the mean y-momentum equation, the following relationships may be established

$$\overline{\frac{p_1}{\rho_1}\Big|_\eta} = \overline{\frac{p_1}{\rho_1}\Big|_{d_1}} + gd_1 = K_1 - \frac{1}{2}\overline{\hat{u}_1^2\big|_{d_1}}, \tag{8}$$

$$\overline{\frac{p_2}{\rho_2}\Big|_\eta} = \overline{\frac{p_2}{\rho_2}\Big|_{-d_2}} - gd_2 = K_2 - \frac{1}{2}\overline{\hat{u}_2^2\big|_{-d_2}}. \tag{9}$$

Our current interest is the deep water case $d_2 \to \infty$ in which case $\overline{\hat{u}_2^2\big|_{-d_2}} \to 0$. We may then choose $K_2 = 0$ so that

$$\overline{\frac{p_1}{\rho_1}\Big|_\eta} = \overline{\frac{p_2}{\rho_2}\Big|_\eta} = 0, \tag{10}$$

$$K_1 = \tfrac{1}{2}\overline{\hat{u}_1^2\big|_{d_1}}. \tag{11}$$

The integral properties of interest are the wave momentum I, the kinetic energy T, the potential energy V, the excess flux of x momentum due to the presence of the wave or radiation stress S, and the x component of the energy flux F. These quantities may be defined as

$$I = I_1 + I_2 = \overline{\rho_1\int_\eta^{d_1}\hat{u}_1\,dy} + \overline{\rho_2\int_{-d_2}^{\eta_1}\hat{u}_2\,dy}, \tag{12}$$

$$T = \frac{1}{2}\rho_1\overline{\int_\eta^{d_1}(u_1^2 + v_1^2)dy} + \frac{1}{2}\rho_2\overline{\int_{-d_2}^{\eta}(u_2^2 + v_2^2)dy} - \tfrac{1}{2}\rho_1\bar{u}_1^2 d_1 - \tfrac{1}{2}\rho_2\bar{u}_2^2 d_2 \tag{13}$$

$$V = \overline{\int_0^\eta(\rho_2 - \rho_1)gy\,dy} = \frac{1}{2}(\rho_2 - \rho_1)g\,\overline{\eta^2}, \tag{14}$$

$$S = \overline{\int_\eta^{d_1}(p_1 + \rho_1 u_1^2)dy} + \overline{\int_{-d_2}^{\eta}(p_2 + \rho_2 u_2^2)dy} - \tfrac{1}{2}g(\rho_2 d_2^2 - \rho_1 d_1^2) - \rho_1\bar{u}_1^2 d_1 - \rho_2\bar{u}_2^2 d_2, \tag{15}$$

$$F = \overline{\int_\eta^{d_1}\left(p_1 + \rho_1 gy + \frac{1}{2}\rho_1(u_1^2 + v_1^2)\right)u_1\,dy} + \overline{\int_{-d_2}^{\eta}\left(p_2 + \rho_2 gy + \frac{1}{2}\rho_2(u_2^2 + v_2^2)\right)u_2\,dy} - \tfrac{1}{2}\rho_1\bar{u}_1^3 d_1 - \tfrac{1}{2}\rho_2\bar{u}_2^3 d_2. \tag{16}$$

The required relationships between the integral properties may be obtained by the use of the momentum equation with (1)–(9) and expansion of the various formulas. The details are straightforward but tedious and we thus quote only the final results:

$$\begin{aligned} 2T &= I_1(c + \bar{u}_1) + I_2(c + \bar{u}_2), \\ S &= 4T - 3V - 2(\bar{u}_1 I_1 + \bar{u}_2 I_2) + d_1\rho_1 K_1 + d_2\rho_2 K_2 \\ &\quad + \tfrac{1}{2}\rho_1\overline{\hat{u}_1^2\big|_{d_1}}d_1 + \tfrac{1}{2}\rho_2\overline{\hat{u}_2^2\big|_{-d_2}}d_2, \\ F &= c(3T - 2V) - 2c(\bar{u}_1 I_1 + \bar{u}_2 I_2) \\ &\quad + c(\tfrac{1}{2}\rho_1\overline{\hat{u}_1^2\big|_{d_1}}d_1 + \tfrac{1}{2}\rho_2\overline{\hat{u}_2^2\big|_{-d_2}}d_2) \\ &\quad + K_1(I_1 + \rho_1\bar{u}_1 d_1) + K_2(I_2 + \rho_2\bar{u}_2 d_2) \\ &\quad + \tfrac{1}{2}\bar{u}_1^2 I_1 + \tfrac{1}{2}\bar{u}_2^2 I_2. \end{aligned} \tag{17}$$

If there is no mean current in either fluid so that $\bar{u}_1 = \bar{u}_2 = 0$, then these expressions agree with those obtained by Hogan,[7] who also included the effects of surface tension.

For the present study there is no loss of generality in taking $\bar{u}_2 = 0$. Putting $d_2 \to \infty$ and using (10)–(11), (17) reduce to

$$\begin{aligned} S &= 4T - 3V - 2\bar{u}_1 I_1 + 2\rho_1 d_1 K_1, \\ F &= c(3T - 2V) - 2c\bar{u}_1 I_1 + \tfrac{1}{2}\bar{u}_1^2 I_1 \\ &\quad + K_1[I_1 + \rho_1 d_1(\bar{u}_1 + c)]. \end{aligned} \tag{18}$$

The quantitites I_1, I_2, V, and K_1 can only be evaluated when (2) is satisfied.

B. Third-order amplitude expansion

The linearized solution of (1)–(3) is

$$\begin{aligned} \eta &= \eta_1\exp(i\theta) + \text{c.c.}, \\ \psi_1 - \bar{u}_1 y &= (c - \bar{u}_1)\eta_1\frac{\sinh k(d_1 - y)}{\sinh kd_1}\exp(i\theta) + \text{c.c.}, \\ \psi_2 - \bar{u}_2 y &= (c - \bar{u}_2)\eta_2\frac{\sinh k(d_2 + y)}{\sinh kd_2}\exp(i\theta) + \text{c.c.}, \end{aligned} \tag{19}$$

where $\theta = k(x - ct)$, $\psi_j (j = 1,2)$ is the stream function in each fluid ($u_j = \partial\psi_j/\partial y, v_j = -\partial\psi_j/\partial x$) and c.c. denotes the complex conjugate. Here $k = 2\pi/\lambda$ is the wavenumber and the phase speed c is given by

$$\rho_2(c - \bar{u}_2)^2 k\coth kd_2 + \rho_1(c - \bar{u}_1)^2 k\coth kd_1 = g(\rho_2 - \rho_1). \tag{20}$$

There are two solutions for c, and we asume that both are real. We shall refer to the larger solution as the upper branch

and the other solution as the lower branch.

This linearized solution for stable waves can be extended to higher order in amplitude by constructing the Stokes expansion. The technique is well known, and in the absence of any mean flow ($\bar{u}_1 = \bar{u}_2 = 0$) the results to third order have been described by Hunt,[10] Thorpe[4] and for the deep fluid case ($d_1, d_2 \to \infty$) by Tsuji and Nagata[11] to the fifth order. In the presence of a mean flow and for the deep fluid case, the third-order expansion has been derived Nayfeh and Saric.[8] We put

$$\eta = \sum_{n=1}^{\infty} \eta_n \exp(in\theta) + \text{c.c.},$$

$$\psi_1 - \bar{u}_1 y = \sum_{n=1}^{\infty} a_n \frac{\sinh nk(d_1 - y)}{\sinh nkd_1} \exp(in\theta) + \text{c.c.}, \tag{21}$$

$$\psi_2 - \bar{u}_2 y = \sum_{n=1}^{\infty} b_n \frac{\sinh nk(d_2 + y)}{\sinh nkd_2} \exp(in\theta) + \text{c.c.},$$

and find that the phase speed is given by, to the third order,

$$\begin{aligned}
&\rho_2(c-\bar{u}_2)^2 kS_2 + \rho_1(c-\bar{u}_1)^2 kS_1 - g(\rho_2 - \rho_1) \\
&\quad = k^3|\eta_1|^2 \Big\{ [\rho_2(c-\bar{u}_2)^2(3S_2^2 - 1) \\
&\qquad - \rho_1(c-\bar{u}_1)^2(3S_1^2 - 1)]^2 \\
&\qquad \times \left[2\left(\frac{\rho_2(c-\bar{u}_2)^2}{S_2} + \frac{\rho_1(c-\bar{u}_1)^2}{S_1}\right)\right]^{-1} \\
&\qquad + 2[\rho_2(c-\bar{u}_2)^2 S_2(2 - S_2^2) + \rho_1(c-\bar{u}_1)^2 S_1(2 - S_1^2)] \Big\},
\end{aligned} \tag{22}$$

where $S_j = \coth kd_j$, $j = 1,2$. It may be shown that if the right-hand side of (22) is positive, then increasing the amplitude $|\eta_1|$ increases the upper branch value of c but decreases the lower branch value; the opposite holds if the right-hand side of (22) is negative. The wave shape can be determined from

$$\begin{aligned}
&\eta_2\left(\frac{\rho_2(c-\bar{u}_2)^2}{S_2} + \frac{\rho_1(c-\bar{u}_1)^2}{S_1}\right) \\
&\quad = \tfrac{1}{2} k\eta_1^2 [\rho_2(c-\bar{u}_2)^2(3S_2^2 - 1) \\
&\qquad - \rho_1(c-\bar{u}_1)^2(3S_1^2 - 1)],
\end{aligned} \tag{23}$$

and

$$\begin{aligned}
&\eta_3\left(\rho_2(c-\bar{u}_2)^2 \frac{S_2}{(3S_2^2+1)} + \rho_1(c-\bar{u}_1)^2 \frac{S_1}{(3S_1^2+1)}\right) \\
&\quad = \frac{1}{8}\eta_2(k\eta_1)\left(\rho_2(c-\bar{u}_2)^2 \frac{(9S_2^4 + 4S_2^2 + 3)}{(3S_2^2+1)}\right. \\
&\qquad \left. - \rho_1(c-\bar{u}_1)^2 \frac{(9S_1^4 + 4S_1^2 + 3)}{(3S_1^2+1)}\right) \\
&\qquad - \frac{1}{4}\eta_1(k\eta_1)^2\left(\rho_2(c-\bar{u}_2)^2 \frac{S_2^3(3S_2^2 - 1)}{(3S_2^2+1)}\right. \\
&\qquad \left. + \rho_1(c-\bar{u}_1)^2 \frac{S_1^3(3S_1^2 - 1)}{(3S_1^2+1)}\right).
\end{aligned} \tag{24}$$

The integral properties can be determined from I_1, I_2, V and K_1, K_2, which to the third order, are given by

$$\begin{aligned}
I_1 &= \rho_1(c-\bar{u}_1)\{2kS_1|\eta_1|^2 + 2k[(S_1^2+1)/S_1]|\eta_2|^2 \\
&\quad + k^2(3S_1^2 - 1)(\eta_2\eta_1^{*2} + \eta_2^*\eta_1^2) \\
&\quad + 2k^3 S_1(S_1^2 - 2)|\eta_2|^4\}, \\
I_2 &= \rho_2(c-\bar{u}_2)\{2kS_2|\eta_1|^2 + 2k[(S_2^2+1)/S_2]|\eta_2|^2 \\
&\quad - k^2(3S_2^2 - 1)(\eta_2\eta_1^{*2} + \eta_2^*\eta_1^2) \\
&\quad + 2k^3 S_2(S_2^2 - 2)|\eta_1|^4\}, \\
V &= g(\rho_2 - \rho_1)(|\eta_1|^2 + |\eta_2|^2), \\
K_1 &= k^2(c-\bar{u}_1)^2(S_1^2 - 1)\{|\eta_1|^2 + \tfrac{1}{4}[(S_1^2 - 1)/S_1^2]|\eta_2|^2 \\
&\quad + (3k/4S_1)(3S_1^2 + 1)(\eta_2\eta_1^{*2} + \eta_2^*\eta_1^2) \\
&\quad + \tfrac{1}{4}k^2(9S_1^2 - 5)|\eta_1|^4\}, \\
K_2 &= k^2(c-\bar{u}_2)^2(S_2^2 - 1)\{|\eta_1|^2 + \tfrac{1}{4}[(S_2^2 - 1)/S_2^2]|\eta_2|^2 \\
&\quad - (3k/4S_2)(3S_2^2 + 1)(\eta_2\eta_1^{*2} + \eta_2^*\eta_1^2) \\
&\quad + \tfrac{1}{4}k^2(9S_2^2 - 5)|\eta_1|^4\},
\end{aligned} \tag{25}$$

where η_j^* is the complex conjugate of η_j. From the form of these expressions we expect them to be useful when $|k\eta_1|^2 \ll 1$ and when $|\eta_1| \ll d_1, d_2$.

III. NUMERICAL SOLUTION OF THE FREE BOUNDARY PROBLEM

A. Formulation of the integral equation

We now restrict attention to the deep water case $d_2 \to \infty$ with $\bar{u}_2 = 0$ and introduce the Boussinesq approximation. To solve the nonlinear boundary value problem on $\mathscr{C}$ it is convenient to work in a frame at rest with respect to the progressive wave. Using (7) the appropriate form of (3) may then be expressed as

$$\begin{aligned}
&(p_j/\rho_j) + gy + \tfrac{1}{2}(u_j - c)^2 + v_j^2 \\
&\quad = K_j + \tfrac{1}{2}c^2 + \tfrac{1}{2}\bar{u}_j(\bar{u}_j - 2c), \quad j = 1,2.
\end{aligned} \tag{26}$$

We define the Boussinesq parameter α and the length, L, time T and density ρ scales as

$$\begin{aligned}
&\alpha = (\rho_2 - \rho_1)/(\rho_2 + \rho_1), \quad \rho = \tfrac{1}{2}(\rho_1 + \rho_2), \\
&L = \lambda/\pi, \quad T = (L/\alpha g)^{1/2}.
\end{aligned} \tag{27}$$

Further we let the quantities P_j, Φ_j, Λ_j, (U_j, C), $j = 1,2$, and (X, Y) be dimensionless forms of $p_j, \phi_j, K_j, (u_j c)$, $j = 1,2$, and (x, y), respectively, with respect to these scales. Using (27) and noting that $\bar{U}_2 = 0$ and $\Lambda_2 = 0$, Eq. (26) may be written in fluids 1 and 2, respectively, as

$$\begin{aligned}
\alpha P_1 = &-(1-\alpha)[\tfrac{1}{2}\alpha(\nabla\Phi_1)^2 + Y] \\
&+ \alpha(1-\alpha)[\Lambda_1 + \tfrac{1}{2}C^2 + \tfrac{1}{2}\bar{U}_1(\bar{U}_1 - 2C)],
\end{aligned} \tag{28a}$$

$$\alpha P_2 = -(1+\alpha)[\tfrac{1}{2}\alpha(\nabla\Phi_2)^2 + Y] + \alpha(1+\alpha)\tfrac{1}{2}C^2. \tag{28b}$$

The pressure condition in the Boussinesq limit may now be expressed by equating the right-hand sides of (28) for a point on $\mathscr{C}$ and taking the limit $\alpha \to 0$. Since the flow is steady, the second condition in (2) (kinematic condition) is that the normal component of the velocity field vanish on $\mathscr{C}$. Hence (2) becomes

$$\left.\begin{aligned} &\tfrac{1}{2}[(\nabla\Phi_2)^2-(\nabla\Phi_1)^2]+2Y+\Lambda_1+\tfrac{1}{2}\bar{U}_1(\bar{U}_1-2C)=0,\\ &\frac{\partial\Phi_j}{\partial n}=0,\quad j=1,2 \end{aligned}\right\}\ \text{on } \mathscr{C}, \tag{29}$$

where n is the local normal direction for a point on $\mathscr{C}$.

We now comment briefly on the use of the rigid boundary model of the free surface $Y=D=d_1/L$. It is easily shown by a first-order linearized analysis of interfacial waves in the presence of a free surface, that the ratio of amplitudes of the free surface to the interfacial motion vanishes as $\alpha\to 0$. While we offer no formal proof, it seems clear on physical grounds that this behavior must also be characteristic of fully nonlinear waves, except possibly for very large waves which nearly reach to the free surface. The reason is that with the scaling (27), chosen as appropriate for interfacial waves, it is readily shown that the displacement of a free surface at $Y=D$ is $O(\alpha)$ and so vanishes as $\alpha\to 0$ (see Grimshaw[12]). Of course this scaling precludes the existence of a wave on the free surface whose dimensionless phase speed is $O(\alpha^{-1/2})$ as $\alpha\to 0$ with the present scaling.

The quantities Φ_1 and Φ_2 may be readily constructed by introducing the complex potential W, physical plane variable Z and cumulative circulation Γ defined by

$$W=\Phi+i\Psi,\quad Z=X+iY,$$
$$\Gamma=\Phi_2-\Phi_1+\text{const.} \tag{30}$$

The technique is related to that developed by Pullin[13] in calculating interfacial instabilities. If we specify the shape of $\mathscr{C}$ by $z(\Gamma)=X_c(\Gamma)+Y_c(\Gamma)$, over a wavelength $\pi\geqslant X\geqslant 0$ then an expression for the complex velocity dW/dZ in the X-wise periodic flow which automatically satisifes (1) on $Y=D$ and also $\partial\Phi/\partial X=-C$, $Y\to-\infty$ ($\bar{U}_2=0$) is given by

$$\frac{dW}{dZ}=\frac{1}{2\pi i}\int_{\mathscr{C}}[\cot(Z-z')-\cot(Z-z^{*\prime}-2iD)]d\Gamma'-C, \tag{31}$$

where z^* is the complex conjugate of z. The first integral is a superposition of vortex-like singularities on $\mathscr{C}$, and the second is its image in $Y=D$. Letting $\Delta\Gamma$ denote the change of Γ in $\pi\geqslant X\geqslant 0$ application of (4) to (31) then shows that

$$\Delta\Gamma=-\pi\bar{U}_1. \tag{32}$$

Equations (29) may be expressed in compact form by noting that on $\mathscr{C}$

$$(\nabla\Phi_1)^2-(\nabla\Phi_2)^2=2\frac{\partial\Gamma}{\partial s}\frac{dW}{ds},$$

where s denotes arclength. Substituting this result into (29) then yields the complex nonlinear integral equation for $z(\Gamma)$

$$\frac{1}{2}\left(\frac{d\Gamma}{dz^*}\right)\left(\frac{dW}{dz}\right)_p+Y_c+\frac{1}{2}\left(\Lambda_1+\frac{1}{2}\bar{U}_1(\bar{U}_1-2C)\right)=0. \tag{33}$$

In Eq. (33), $(dW/dz)_p$ refers to the mean of the limiting values of (31) obtained where $Z\to z(\Gamma)$ from either side of $\mathscr{C}$. Hence the first integral in (31) is a Cauchy Principle Value (CPV) integral. For given D and $\bar{U}_1$ (33) must be satisfied on $\mathscr{C}$. Two additional constraints however are required to determine the unknown parameters C and Λ_1, and are provided by

$$\int_{\mathscr{C}}Y_c\frac{\partial X_c}{\partial s}\,ds=0, \tag{34a}$$
$$Y_{c_{\max}}-Y_{c_{\min}}=2\delta, \tag{34b}$$

expressing, respectively, the requirements that the x axis be the mean level of $\mathscr{C}$ ($\bar{\eta}=0$) and that the wave amplitude be δ.

B. Small-amplitude solution

The small-amplitude solution to (33) may be obtained directly from an expansion of (33) in powers of δ or from the analysis outlined in Sec. IIB. The dispersion relationship (22) in the Boussinesq approximation and with $\bar{U}_2=0$, $d_2\to\infty$ becomes in the present dimensionless coordinates,

$$C=C_0+\delta^2C_1+O(\delta^4), \tag{35a}$$

where

$$C_0=\frac{\bar{U}_1\coth 2D\pm[1+\coth 2D(1-\bar{U}_1^2)]^{1/2}}{1+\coth 2D} \tag{35b}$$

$$C_1\{\pm[1+\coth 2D(1-\bar{U}_1^2)]^{1/2}\}=\frac{[2C_0^2-(C_0-\bar{U}_1)^2(3\coth^2 2D-1)]^2}{4[C_0^2+(C_0-\bar{U}_1)^2\tanh 2D]}+[C_0^2+(C_0-\bar{U}_1)^2\coth 2D(2-\coth^2 2D)]. \tag{35c}$$

Note that when the right-hand side of (35c) is positive, then for the upper (lower) branch solution, C_1 is positive (negative). The opposite holds if the right-hand side of (35c) is negative. There are no steady progressive wave solutions if

$$\bar{U}_1^2>U_c^2=1+\tanh(2D). \tag{36}$$

From (36) it may be shown that for fixed d_1 and $\hat{U}=\bar{U}_1/(\alpha g d_1/\pi)^{1/2}>0$ there exists a wavenumber $k_s=2\pi\epsilon/d_1$ above which no progressive wave-like solution exists where ϵ is the solution of

$$\hat{U}^2\epsilon=1+\tanh(2\pi\epsilon).$$

Hence, the first-order stability theory predicts unlimited instability of the interface at sufficiently high k except when $\hat{U}=0$.

The wave shapes to third order are given by

$$\hat{\eta}=2|\hat{\eta}_1|\cos 2X+2|\hat{\eta}_2|\cos 4X+2|\hat{\eta}_3|\cos 6X+\ldots, \tag{37}$$

where here $\hat{\eta}_{1-3}$ are dimensionless forms of η_{1-3}. In the present case $\bar{U}_2=0$ and $\rho_1=\rho_2$ (Boussinesq approximation); $S_2=1, S_1=\coth 2D$ and $k=2$. From (34b) $\delta=2|\hat{\eta}_1|+2|\hat{\eta}_3|$. Dimensionless forms of the integral invariants to third order may be readily obtained from (25).

C. Numerical solution

Numerical solutions to (33) were obtained by two quite different techniques. In the first [segment midpoint approxi-

mation (SMA method)] we break $\mathscr{C}$ into $2N$ straight segments with end point (Γ,z) coordinates defined by

$$\Gamma_j,z_j = z_{j-1} + \Delta a w_j e^{i\theta_j}, \quad j = 1...2N. \tag{38}$$

In (38) $\Delta a w_j$ is the chord length for the jth segment, Δa is a dummy parameter on $\mathscr{C}$, θ_j is the tangent angle to the X axis and $z_0 = 0 + iY_{c_0}$. The arc length weights w_j are a known function of j and are introduced in order to allow use of small chord length increments in regions of high interface curvature. An approximation to (31) was obtained assuming a linear variation of $z(\Gamma)$ and integrating analytically within each segment $\Gamma_j \geqslant \Gamma > \Gamma_{j-1}, j = 1...2N$. A discretized form of the integral equation was then formulated by satisfying (33) at the mid point of the segments $j = 1...N$ (allowed by assuming symmetry of the wave profile about its crest) using a simple first-order difference approximation to $d\Gamma/dz^*$ and taking due care in evaluating the CPV contribution to the integral. For given $\bar{U}$, D and δ this provides $2N$ equations for the $2N+4$ unknown quantities $\Delta\Gamma_j,\theta_j, j = 1...N; \Delta a, Y_{c_0}, \Lambda_1$, and C. The four closure equations are obtained by differenced approximations to (32) and (34a) and the requirement from (34b) that $z_N - z_0 = \pi/2 - 2i\delta$. The $2N+4$ nonlinear equations were solved using a Newton–Raphson iterative technique based on analytical evaluation of the Jacobian. For $N = O(10^2)$ the required CPU time per solution varies as $O(N^2)$.

While generally satisfactory the SMA method was found to yield inaccurate values of the $O(\delta^2)$ quantity $C - C_0$ for $\delta \sim 0.1D$. Hence it was complemented by the second Fourier expansion (FE) technique (Saffman and Szeto[14]) which may be regarded as the numerical equivalent of the Stokes expansion. Here we rewrite (33) and (31) as

$$\frac{1}{2}\gamma(a)\left(\frac{\partial z^*}{\partial a}\right)^{-1}\left(\frac{dW}{dz}\right)_p + Y_c + \frac{1}{2}\left(\Lambda_1 + \frac{1}{2}\bar{U}_1(\bar{U}_1 - 2C)\right) = 0 \tag{39}$$

$$\left(\frac{dW}{dz}\right)_p = \frac{1}{2\pi i}\int_{\pi/2}^{-\pi/2} [\cot(z - z') - \cot(z - z^{*\prime} - 2iD)] \times \gamma(a')da' - C, \tag{40}$$

where $\pi \geqslant a \geqslant 0$ and $\gamma = \partial\Gamma/\partial a$. We now expand $z(a)$ and $\gamma(a)$ as

$$z(a) = a + \sum_{n=0}^{N-1} [A_n \sin(2na) + iB_n \cos(2na)], \tag{41a}$$

$$\gamma(a) = -\bar{U} + \sum_{n=1}^{N} E_n \cos(2na), \tag{41b}$$

noting that (41b) satisfies (32) automatically. The A_n may be chosen to give any desired distribution of $\mathrm{Re}[z(a)]$ on $\mathscr{C}$. The unknowns are here the $2N+2$ quantities $B_n, n = 0...N-1, E_n, n = 1...N, \Lambda_1$, and C. Of the required equations $2N-2$ are obtained by satisfying (39) for $a_j = j\pi/(2N), j = 1...N-1$ and two are provided by satisfying the real part of (39) at $a_0 = 0$ and $a_N = \pi/2$ (wave crest and trough), the imaginary part vanishing identically. Here (40) was calculated at a_j by subtraction out and analytical treatment of the singular/strongly varying parts of the first/second terms (see Appendix) and evaluation of the residual well behaved integrals by the accurate trapezoidal rule for periodic functions. The two closure equations follow by substitution of (41a) into (34). Again a Newton–Raphson solution method was utilized but here for $N = O(10^2)$, the CPU time per solution varies as N^3.

IV. RESULTS AND DISCUSSION

For specified $N,\bar{U}_1,D$, and a given branch, SMA and FE solutions were obtained by initially using the $O(\delta)$ Stokes solution as an initial approximation for small δ. Subsequent solutions were then obtained by incrementing δ in small intervals $\Delta(\delta)$ until a value was reached where the iteration scheme diverged. The last used $\Delta(\delta)$ was then halved and the strategy continued until $\Delta(\delta) = O(D/100)$ at which point the search for the highest wave corresponding to the maximum δ was halted. A value $N = 77$ was used for all SMA method calculations which were performed on a Cyber 72 computer. For the FE computations N varied with δ with minimum and maximum values of $N = 38$ and $N = 75$, respectively. These results were obtained in single precision mode on a VAX 11/780 machine.

Integral properties were calculated by expressing I_1, I_2 and V in dimensionless form as

$$\hat{I}_1 = -\frac{1}{\pi}\int_{\mathscr{C}} Y_c\left[\left(\frac{dW}{dz}\right)_p\left(\frac{\partial z}{\partial a}\right) - \frac{1}{2}\gamma\right]da,$$

$$\hat{I}_2 = \frac{1}{\pi}\int_{\mathscr{C}} Y_c\left[\left(\frac{dW}{dz}\right)_p\left(\frac{\partial z}{\partial a}\right) + \frac{1}{2}\gamma\right]da,$$

$$\hat{V} = \frac{1}{\pi}\int_{\mathscr{C}} Y_c^2\frac{\partial X_c}{\partial a}da. \tag{42}$$

The integrals were evaluated using the periodic function trapezoidal rule and $\hat{T},\hat{S}$, and $\hat{F}$ were calculated from (18). Tables I(a)–(b) compare values of some wave properties presently obtained with the results of Holyer[5] calculated by a 31 term Stokes expansion. The FE method with $N = 38$ gives results in agreement to four and five digits with the 31 term Stokes expansion at $\delta = 0.1$ while the third-order expansion is accurate to four digits. The SMA computation of $C - C_0$ is in error by a factor of two, possibly because of discretization

TABLE I. Comparison of present results with those of Holyer (1979). (a) $\bar{U}_1 = 0, D \to \infty, \delta = 0.1$. (b) $\bar{U}_1 = 0, D \to \infty, \delta = 0.55$.

(a)	Holyer (1979)	Third-order Stokes	FE numerical $N = 38$	SMA numerical $N = 77$
$(C - C_0)\times 10^2$	0.710 6	0.707 1	0.711 0	0.389
$\hat{I}\times 10$	0.142 829	0.142 801	0.142 824	0.1433
$\hat{V}\times 10^2$	0.504 985	0.504 981	0.504 963	0.5047

(b)	Holyer (1979)	Third-order Stokes	FE numerical $N = 55$	SMA numerical $N = 77$
$C - C_0$	0.243 3	0.214 0	0.247 6	0.246 8
$\hat{I}$	0.561 1	0.442 5	0.568 2	0.5693
$\hat{V}$	0.201 8	0.200 5	0.203 5	0.2033

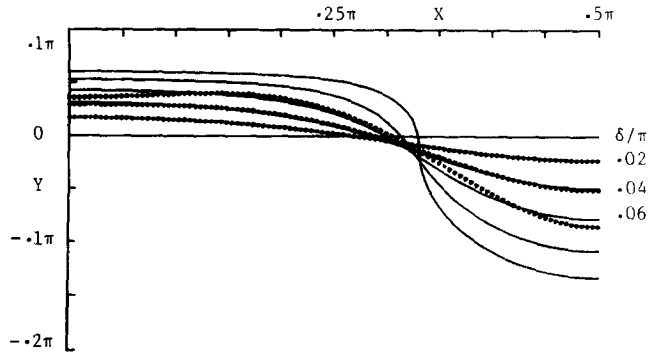

FIG. 1. Wave profiles, $D/\pi = 0.1$, $\bar{U}_1 = 0$. ——numerical, $\delta/\pi = 0.2, 0.4, 0.6, 0.8, 0.963\times10^{-1}$.....third-order Stokes expansion; values of δ/π as indicated.

errors at small δ where the imaginary part of (33) (which determines C) is the difference between order δ^2 quantities. For the near highest wave amplitude $\delta = 0.55$ however, differences between FE and SMA method predictions are generally confined to the fourth figure but there are consistent third figure differences compared to the 31 term Stokes expansion. This is perhaps because the boundary conditions in the expansion are satisfied on $Y = 0$ which may introduce errors even at very high order.

Other calculations were carried out for the most part with $D/\pi = 0.1$ and 0.01 which is typical of the thermocline application. Selected wave profile shapes shown in Figs. 1–6 are SMA results but since these generally agreed with FE method profiles to three digits (except near the highest wave) the respective shapes are identical on the scale displayed. For $D\to\infty$, Holyer conjectured that the highest wave is determined by the condition that the fluid velocity at some point on the wave profile should equal the wave phase speed, or equivalently, that the wave profile should develop a vertical section. Thus S-shaped waves (those with a portion of the interface with three values of Y for given X) are specifically excluded. While the SMA method should be capable of calculating such waves if they exist, we find that for the present configuration the highest calculated wave conforms either to Holyer's condition or to the additional constraint that the height of the wave crest must not exceed D. Thus in Figs. 1, 2, and 4, local infinite profile slope is the limiting condition reached while in Figs. 3(a) and 5–6, the highest possible wave

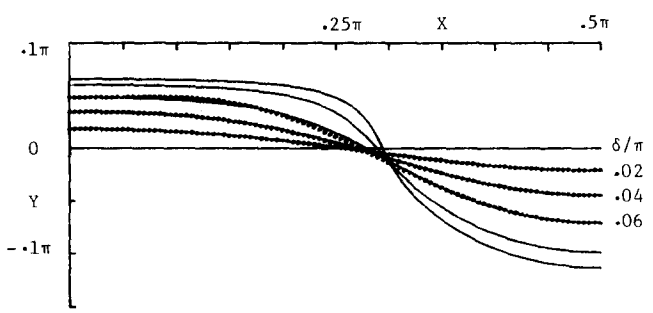

FIG. 2. Wave profiles, $D/\pi = 0.1$, $\bar{U} = 0.2$, upper branch, ——numerical, $\delta/\pi = 0.2, 0.4, 0.6, 0.8, 0.9\times10^{-1}$. ....third-order Stokes expansion; values of δ/π as indicated.

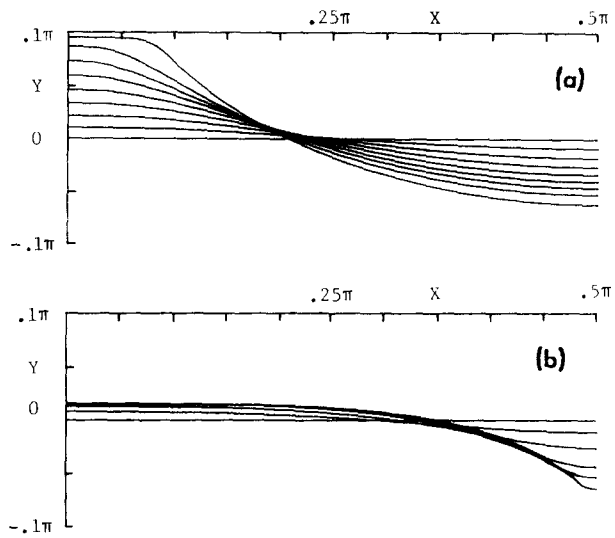

FIG. 3. (a)Wave profiles, $D/\pi = 0.1$, $\bar{U}_1 = 1.0$, upper branch, $\delta/\pi = 0.1$, 0.2, 0.3, 0.4, 0.5, 0.6, 0.7, 0.788×10^{-1}. (b) Wave profiles, $D/\pi = 0.1$, $\bar{U}_1 = 1.0$, lower branch, $\delta/\pi = 0.1$, 0.2, 0.3, 0.35, 0.4×10^{-1}.

is clearly determined by the free surface ceiling. The highest wave profiles for ceiling constrained waves (particularly that in Fig. 5) suggests a limit solution in which the upper layer becomes disconnected and forms an infinite array of half-oval-shaped dead-fluid regions each with horizontal top on the plane $Y = D$. Of course, in any application of these results to the ocean thermocline, the assumption of the present model that the ocean free surface can be modeled with a rigid plane will be a severe limitation for those cases where the wave reaches that level. Figures 1 and 2 also show third-order Stokes expansion wave profiles. For $\delta/\pi = 0.02$ these are indistinguishable from the corresponding numerical results but discrepancies appear at higher amplitude.

Some profile shapes show solitary-wave features with long flat crests and narrow peaked troughs. Generally this characteristic is associated with low shear ($\bar{U}_1 = 0$,0.2) and is more marked for longer waves when $D/\pi = 0.01$. The Stokes expansion will be valid for $|k\eta_1|^2 \ll 1$ and $|\eta_1| \ll d$; the latter condition gives a restraint. In fact the nonlinear long wave regime is entered when $\eta_1 \sim kd^2 (\hat{\eta}_1 \sim 2D^2)$ a condition which is satisfied with $\hat{\eta}_1 \sim O(10^{-3})$ when $D/\pi = 0.01$ but

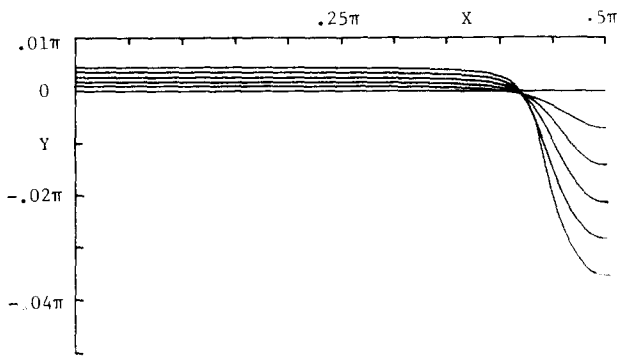

FIG. 4. Wave profiles $D/\pi = 0.01$, $\bar{U}_1 = 0$. $\delta/\pi = 0.4$, 0.8, 1.2, 1.6, 2.0×10^{-2}.

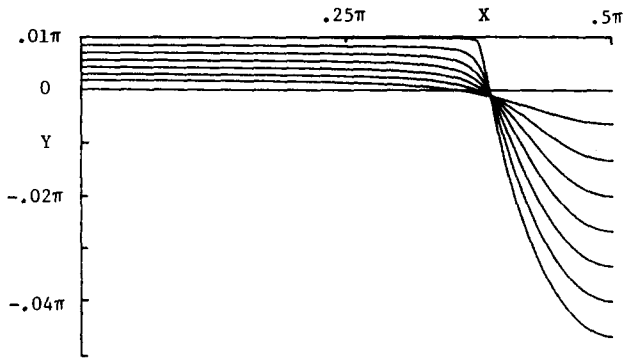

FIG. 5. Wave profiles, $D/\pi = 0.01$, $\overline{U}_1 = 0.2$, upper branch, $\delta/\pi = 0.4, 0.8, 1.2, 1.6, 2.0, 2.4, 2.8\times10^{-2}$.

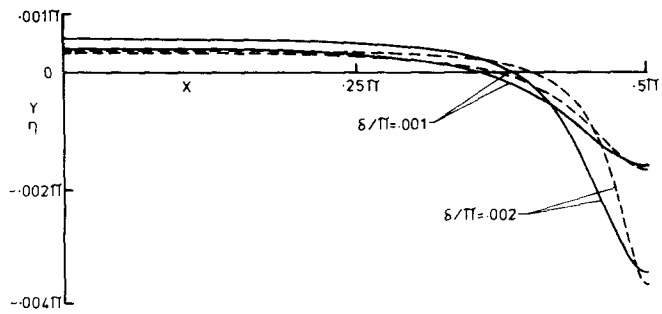

FIG. 7. Wave profiles, $D/\pi = 0.01$, $\overline{U}_1 = 0$, ——present numerical, – – –Benjamin's[15] analytic solution for long periodic waves.

$O(10^{-1})$ when $D/\pi = 0.1$. This suggests that for $D/\pi = 0.01$ the third-order Stokes expansion is only valid for very small amplitudes, say $O(10^{-4})$. This conjecture was verified by generally excellent agreement with the FE method predictions at $\delta/\pi \sim O(10^{-4})$ but very rapid divergence when $\delta/\pi = O(10^{-3})$. An exception was for $\overline{U}_1 = 0.2$, lower branch ($C_0 = -0.0502$) where nonlinear effects in the numerical solutions were found to be significant for $\delta/\pi \geqslant 5\times10^{-5}$, while in the Stokes expansion $|\hat{\eta}_3|$ exceeded $|\hat{\eta}_1|$ over approximately the same range. This behavior may be associated with near zero C ($C_0 = 0$ at $\overline{U}_1 = [\tanh(2D)]^{1/2}$, lower branch) for long waves.

A more apropriate comparison for $D/\pi = 0.01$ is perhaps with Benjamin's[15] periodic solution for long waves in deep fluids, the wave shape and phase speed of which are given in the present coordinates by

$$Y = \delta \sinh p\left(1 - \frac{\sinh p}{\cosh p + \cos(2X)}\right), \tag{43a}$$

$$C = (2D)^{1/2} + (2D)^{3/2}(\tfrac{1}{2}\coth p - 1), \tag{43b}$$

where $\sinh p = 4D^2/3\delta$. In the comparison with the present results shown in Fig. 7 there is some discrepancy in the detailed profile shapes but the qualitative similarity is quite evident. For $D = 0.01\pi$ and $\delta = 0.001\pi$, 0.002π, Eq. (43b) gives $C = 0.2553$ and 0.2733, respectively compared with corresponding 38 term FE numerical values of $C = 0.2528$ and 0.2658.

The variation of integral and other wave properties with wave amplitude are shown in Figs. 8–12. The numerical results show excellent agreement with the third-order Stokes expansion at low δ/π with reasonable agreement for some quantities over the whole amplitude range. Numerical SMA and FE predictions of integral properties generally agreed to three figures while results for $C - C_0$ usually agreed to $O(10^{-3})$ at moderate δ/π with divergence at $\delta \sim O(D/10)$, where $\delta^2 \sim O(10^{-3})$ for $D/\pi = 0.1$. One notable exception was for $D/\pi = 0.01$, $\overline{U}_1 = 1.0$, where SMA and FE predictions of $C - C_0$ were always $O(10^{-3})$ and (10^{-4}), respectively, with $C_0 = 1.0$. Hence $C - C_0$ is not shown in Fig. 12. Lower branch values of $\hat{I}$, $\hat{S}$, and $\hat{F}$ for $d/\pi = 0.1$, $\overline{U}_1 = 1.0$ may be seen to be negative in Fig. 10(b) indicating that the flux of mass, momentum and energy actually decrease in the presence of the wave. This was found to be generally charac-

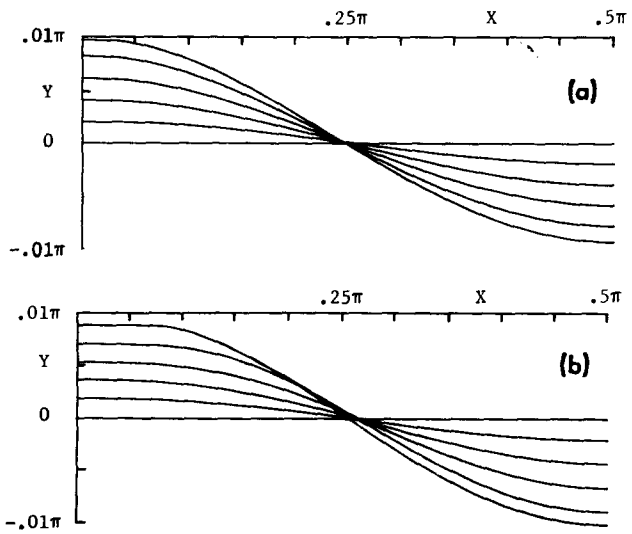

FIG. 6. (a) Wave profiles, $D/\pi = 0.01$, $\overline{U}_1 = 1.0$, upper branch, $\delta/\pi = 0.2, 0.4, 0.6, 0.8, 0.95\times10^{-2}$. Wave profiles, $D/\pi = 0.01$, $\overline{U}_1 = 1.0$, lower branch, $\delta/\pi = 0.2, 0.4, 0.6, 0.8, 0.95\times10^{-2}$.

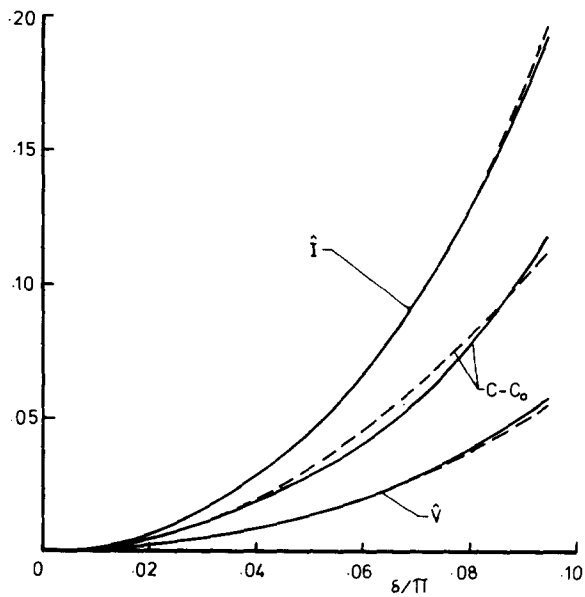

FIG. 8. Integral properties of waves, $D/\pi = 0.1$, $\overline{U}_1 = 0$. ——numerical, – – –third-order Stokes expansion.

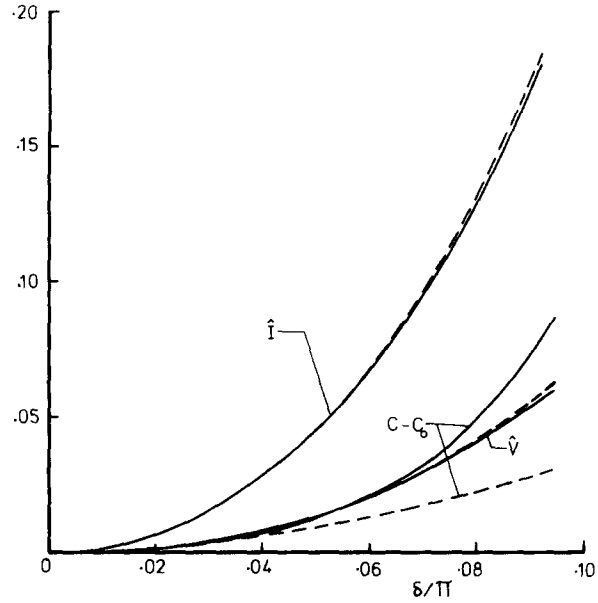

FIG. 9. Integral properties of waves, $D/\pi = 0.1$, $\overline{U}_1 = 0.2$, upper branch, ——numerical, – – –third-order Stokes expansion.

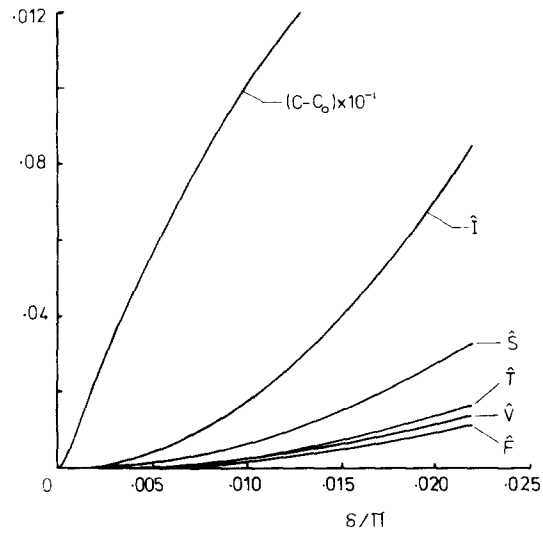

FIG. 11. Integral properties of waves, $D/\pi = 0.01$, $\overline{U}_1 = 0$. Numerical only.

teristic of lower branch solutions. For all solutions obtained, the integral properties showed a monotonic increase with amplitude up to the highest wave.

V. CONCLUSIONS

We have obtained numerical solutions for nonlinear progressive internal waves near a free surface in a two-layer inviscid Boussinesq fluid. For small values of the ratio of the upper layer thickness to wavelength the calculated waves profiles showed strong nonlinear features. Solitary-wave-like behavior was exhibited for some cases with corresponding wave amplitudes exceeding the upper layer thickness. Upper and lower branch solutions with different profile shapes and wave integral properties were obtained for cases in which there existed finite mean velocity difference across the density interface.

In view of the linear instability of the present model at small wavelength it seems almost certain that solutions obtained for nonzero mean velocity difference would exhibit strong Kelvin–Helmholtz instability. Stability may be possible with the introduction of a surface tension term (see Vanden-Broeck[6]) which would be quite straightforward in the present model. The physical relevance of a surface tension mechansim in the thermocline application however is rather questionable. The stability of the solitary wave-like solutions

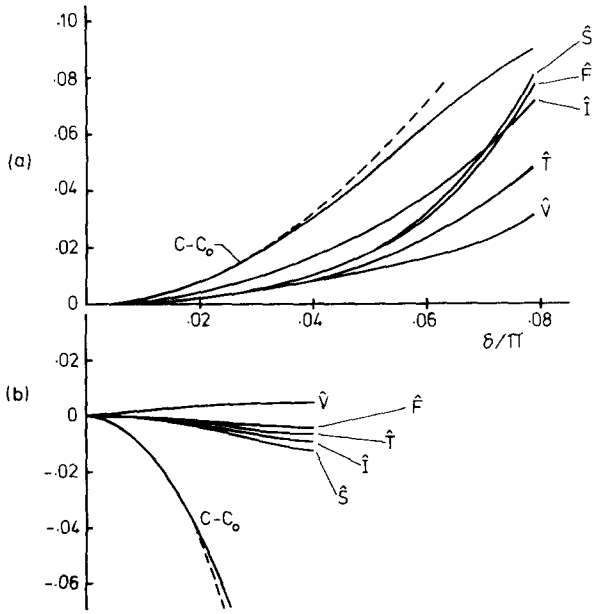

FIG. 10. Integral properties of waves $D/\pi = 0.1$, $\overline{U}_1 = 1.0$, (a) upper branch, (b) lower branch, ——numerical, – – –third-order Stokes expansion $(C - C_0)$.

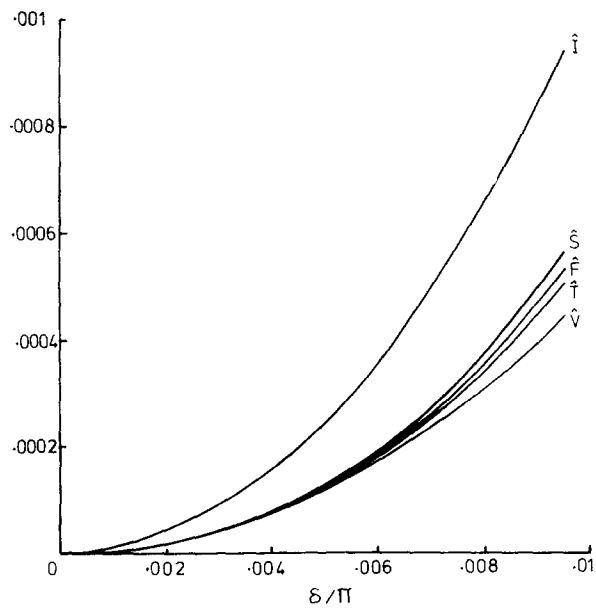

FIG. 12. Integral properties of waves, $D/\pi = 0.01$, $\overline{U}_1 = 1.0$. Upper branch, numerical only.

obtained with zero velocity difference remains an open question and clearly requires further study.

APPENDIX: EVALUATION OF THE INTEGRALS

The calculation of (31) using a piecewise linear representation of $z(\Gamma)$ is straightforward and is not further discussed. The first (CPV) integral I_1 in (40) was evaluated by writing it as

$$I_1 = \frac{1}{2\pi i}\int_{\mathscr{C}} \cot(z - z')\gamma'\, da'$$
$$= \frac{1}{2\pi i}\int_{\mathscr{C}} \cot(z - z')\left[\gamma' - \gamma\left(\frac{\partial z}{\partial a}\right)^{-1}\left(\frac{\partial z'}{\partial a'}\right)\right] da'$$
$$+ \gamma\left(\frac{\partial z}{\partial a}\right)^{-1}\frac{1}{2\pi i}\int_{\mathscr{C}} \cot(z - z')dz'. \tag{A1}$$

For a point on $\mathscr{C}$, the second integral in (A1) vanishes identically. The first integrand now has an analytic smoothly varying integrand which takes the value

$$\gamma\left(\frac{\partial^2 z}{\partial a^2}\right)\left(\frac{\partial z}{\partial a}\right)^{-2} - \left(\frac{\partial \gamma}{\partial a}\right)\left(\frac{\partial z}{\partial a}\right)^{-1}$$

as $a \to a'$. The second integral in (40) is not singular but for small D the integrand varies rapidly near $a' = a$. It may be decomposed as in (A1) and the rapidly varying part evaluated analytically to yield

$$I_2 = -\frac{1}{2\pi i}\int_{\mathscr{C}} \cot(z - z^{*\prime} - 2iD)$$
$$\times\left[\gamma' - \gamma\left(\frac{\partial z^*}{\partial a}\right)^{-1}\left(\frac{\partial z^{*\prime}}{\partial a'}\right)\right] da' - \frac{1}{2}\gamma\left(\frac{\partial z^*}{\partial a}\right)^{-1}. \tag{A2}$$

The integrals in (A1) and (A2) are now in a form suitable for calculation using the periodic-function trapezoidal rule.

[1] D. Halpern, J. Mar. Res. **29**, 116 (1970).
[2] D. M. Farmer, J. Phys. Ocean. **8**, 63 (1978).
[3] D. R. Cristie, K. J. Muirhead, and A. L. Hales, J. Atmos. Sci. **35**, 805 (1978).
[4] S. A. Thorpe, Phil. Trans. R. Soc. London Ser. A **263**, 563 (1968).
[5] J. Y. Holyer, J. Fluid Mech. **93**, 433 (1979).
[6] J. Vanden-Broeck, Phys. Fluids **23**, 1723 (1980).
[7] S. J. Hogan, Phys. Fluids **24**, 774 (1981).
[8] A. H. Nayfeh and W. S. Saric, J. Fluid Mech. **55**, 311 (1972).
[9] S. A. Thorpe, J. Fluid Mech. **85**, 7 (1978).
[10] J. N. Hunt, La Houille Blanch **4**, 515 (1981).
[11] Y. Tsuji and Y. Nagata, J. Oceanogr. Soc. Jpn. 61 (1973).
[12] R. H. J. Grimshaw, J. Fluid Mech. **86**, 415 (1978).
[13] D. I. Pullin, J. Fluid Mech. **119**, 507 (1982).
[14] P. G. Saffman and R. Szeto, Phys. Fluids **23**, 2339 (1980).
[15] T. Brooke-Benjamin, J. Fluid Mech. **29**, 559 (1966).